Activity-induced mixing and phase transitions of self-propelled swimmers

Pallab Sinha Mahapatra*
Department of Mechanical Engineering, Indian Institute of Technology Madras, Chennai, India

Sam Mathew
Gyan Data Pvt. Ltd., IIT Madras Research Park, Chennai, India

(Received 5 May 2018; published 18 January 2019)

We study the mixing of active swimmers. Two different types of swimmers (modeled as particles) are placed initially in two boxes with an interconnection between them. The mixing of swimmers happens as they move with their own self-propelled forces. The self-propelled force is constant and the direction of the exerted thrust is governed by the neighboring swimmers. Overall mixing of the swimmers depends on the magnitude of the exerted thrust, the initial packing fraction, and the activity level. Different nonequilibrium states are also identified depending on the exerted thrust and the initial packing fraction of the swimmers.

DOI: 10.1103/PhysRevE.99.012609

I. INTRODUCTION

Independently moving swimmers can show interesting collective behavior. As these swimmers propel themselves, they are often called self-propelled swimmers or self-propelled particles. The collective motion of the self-propelled swimmers are commonly observed in flocks of birds, schools of fish [1], human crowds [2], bacterial colonies [3], different cells [4], etc. Collective behavior is also common in the dense active particle system [5–9].

Researchers have identified global patterns in the self-propelled system through experimental, numerical, and theoretical studies. Large-scale nonequilibrium behavior of the active particles was observed by Baskaran and Marchetti [10]. Phase transitions in confined domains have been observed for dense active colloids [6] or soft active particles [11,12]. Self-propelled systems have exhibited different phases due to changes in the activity of the particles [12] or depending on the initial packing fraction [6]. These include thermal motion, solid, or gaslike phases. For highly viscous fluids the common phases observed are "coherent flock," "rigid rotation," and "random droplet" [13]. Phase transitions of microswimmers due to flagellar movement and confined geometry were reported by Tsang and Kanso [14]. They identified three phases: "chaotic swirling," "stable circulation," and "boundary aggregation." In the last two decades, there has been a huge amount of research focused on self-propelling particles and the dynamics of their motion. As a result, researchers have defined various models to this end. The most popular models are the Czirók model [15], the Boids flocking model [16], the Vicsek original model [17], the Vicsek modified model, etc. Among all the models, the Vicsek model [17] is the most studied model for collective dynamics. According to this model, the self-propelled particles are aligned with their neighbors, which are present inside the "influence zone" due to some constant "angular noise." In the self-propelled system noise arises due to the "thermal Brownian motion," due to "hydrodynamic interactions" or because of the "intrinsic fluctuations" of the individual agents [18]. The effect of noise on the alignment of the self-propelled rods was studied by Ginelli *et al.* [19]. They have shown that different phases can be observed depending on the magnitude of the white noise. Collective behavior or sometimes phase separation [20] was observed using the Vicsek model as well as without having any alignment mechanism [21]. Many variants of the Vicsek model were discussed earlier [22–24].

The self-propelled motion of the individual particles (or swimmers) induces long-range velocity fields, which creates the bulk motion in the liquid medium [25]. From various experiments [26–28] and numerical simulations [29,30] it has been found that the self-propelled swimmers can enhance the diffusion mixing. Mixing of the surrounding liquid due to the movement of the swimmers, also called biomixing [30], is very relevant for the vertical mixing in the ocean [31]. Self-propelled swimmers can also be used to enhance mixing inside the micromixer [27]. Sokolov *et al.* [32] experimentally showed that the collective motion of bacteria enhances mixing in dense suspensions. The packing fraction (or concentration) of the swimmers has a significant role in phase transitions and it is unpredictable in many cases [33,34]. Hydrodynamic interactions between the swimmers are very important in the overall mixing of the swimmers. In this work, we are interested in the mixing of the swimmers and not the medium. We have studied the mixing behavior of the self-propelled swimmers kept in two separate boxes. There is only one connecting passage between the two boxes as shown in Fig. 1. The mixing behavior is compared for different coordination forces of the swimmers. The effects of the self-propelled force, the initial packing fraction of the swimmers, and the noise in the system on mixing are also studied. Different global patterns and surprising phase transitions are observed depending on the exerted thrust and the packing fraction of the swimmers. We first describe the modeling approach and

*pallab@iitm.ac.in

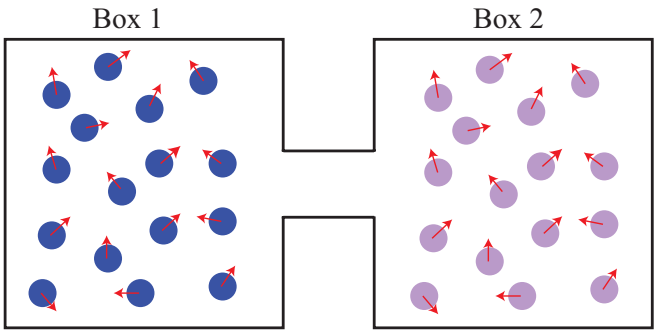

FIG. 1. The definition of the problem is presented. Swimmers are initially in two separate boxes. Initially, there are no swimmers in the connecting path between the two boxes. Particles are colored blue for Box 1 and pink for Box 2. The self-propelled forces of these swimmers are varied to see the effect of activity on mixing.

simulation procedures. Next, we describe the results and show the effect of the coordination coefficient (C_v) and the packing fraction of the swimmers on phase transitions and the mixing index η. An order parameter is defined to identify the different phases.

II. MODELING AND SIMULATIONS

The self-propelled swimmers are generally modeled as discrete particles [12,35,36]. Either overdamped equation of motion [35,37] or force based models [12,36] are used to describe the behavior of the self-propelled particles. In the present work, we have used the discrete particle based methods to model self-propelled systems. Earlier, Levine *et al.* [36] reported that the discrete models agree very well with the continuum flock solutions in both one dimension and two dimensions. In the present work, the swimmers are modeled as soft disks of radius r and mass m. All swimmers are confined in an enclosure and they have a self-propelled force on which they can propel themselves. The force models are similar to our previous work [12,38].

The total force on any jth swimmers $\vec{F}^j$ is the sum of the self-propelled force $\vec{F}^j_{\rm sp}$, the internal (swimmer-swimmer) interaction force $\vec{F}^j_{pp}$, the alignment force $\vec{F}^j_a$, and the frictional force $\vec{F}^j_f$:

$$\vec{F}^j = \vec{F}^j_{\rm sp} + \vec{F}^j_{pp} + \vec{F}^j_a + \vec{F}^j_f + F_{\rm noise}. \tag{1}$$

The self-propelled force $\vec{F}^j_{\rm sp}$ is modeled as [12]

$$\vec{F}^j_{\rm sp} = m_j\left(\beta - \xi\left|\vec{v}^j_p\right|^2\right)\hat{v}^j_p. \tag{2}$$

Here, m_j is the mass of the individual swimmer, $\vec{v}^j_p$ is the instantaneous velocity of the jth swimmer, $\hat{v}^j_p$ is a unit vector in the direction of the velocity, and β is a thrust coefficient. Here, ξ is a small number that restricts the unbounded acceleration of the single swimmer in the dilute suspension limit [39]. As the thrust is modeled as a monopole force, ξ can also be rationalized as a net momentum sink. For dense systems ξ can even be set to zero [12].

The swimmer-swimmer interaction force $\vec{F}^j_{pp}$ is calculated considering the interaction between soft spheres [38]:

$$\vec{F}^j_{pp} = \begin{cases} -k_n\vec{\delta}, & |\vec{\delta}| > 0, \\ \vec{0}, & \text{otherwise.} \end{cases} \tag{3}$$

Here, $\vec{\delta} = \{|\vec{r}_i - \vec{r}_j| - [(d_i + d_j)/2]\}\frac{\vec{r}_i - \vec{r}_j}{|\vec{r}_i - \vec{r}_j|}$ is the distance between two swimmers, i and j. Their position vectors are $\vec{r}_i$ and $\vec{r}_j$ and their diameters are d_i and d_j, respectively.

The alignment force $\vec{F}^j_a$ on the jth swimmer arises because of the relative velocity of the swimmer with the surrounding swimmers. The alignment force is a form of force used earlier [23,36] that helped in aligning the swimmer with the flock. This coordination force not only restricts the swimmers to achieve large speeds but also helps in aligning the swimmers. The alignment force on any swimmer can be estimated as

$$\vec{F}^j_a = C_v d_j\left(\vec{v}^j - \vec{v}^j_p\right). \tag{4}$$

Here, C_v determines the local alignment of the swimmer with the neighboring swimmers. In all our simulations, we have considered C_v as a parameter to understand the effect of the coordination of the swimmers. Here, $\vec{v}^j$ is the weighted average velocity calculated from the n neighboring swimmers of the jth swimmer [38],

$$\vec{v}^j = \frac{\sum_{i=1}^n m_i W_{ij}(\|\vec{r}_i - \vec{r}_j\|, h_j)\vec{v}^i_p}{\sum_{i=1}^n m_i W_{ij}(\|\vec{r}_i - \vec{r}_j\|, h_j)}, \tag{5}$$

where the function W_{ij} is in the Gaussian form,

$$W_{ij} = \begin{cases} \exp\left(-\eta\frac{\|\vec{r}_i - \vec{r}_j\|^2}{{h_j}^2}\right), & \frac{\|\vec{r}_i - \vec{r}_j\|}{h_j} \leqslant 1, \\ 0, & \text{otherwise.} \end{cases} \tag{6}$$

Here, h_j is a cutoff radius of influence for the jth swimmer. h_j corresponds to the influence zone of the swimmers; η is a constant parameter of value 2 [40]. From Eq. (4) it can be said that the alignment force helps in local coordination of the swimmers. It can be understood that random thermal motion will be observed on the swimmers in the absence of any kind of restoring force. The frictional force on any swimmer can be estimated as

$$\vec{F}^j_f = -C_v d_j \vec{v}^j_p. \tag{7}$$

A noise term is added with the total force for each swimmer in addition to the alignment force and the self-propelled force. The white noise term is of the form $C_v d_j \gamma\zeta$, where γ is the noise amplitude and ζ denotes the white noise. The value of $\gamma = 10^{-6}$ is chosen for all the simulations, if not mentioned otherwise.

The simulation domain is shown in Fig. 1. It has been reported earlier [41,42] that the dimensionality of the model has very minimal effect on the results of the collective behavior of the self-propelled systems. We performed the simulation with a two-dimensional setting and each box was a square ($L \times L$). The length of the connector was $0.4 \times L$ and the width was $0.2 \times L$. All swimmers were considered as soft disks of diameter $0.005 \times L$. Initially no swimmers were packed at the connector. We started the simulation with zero initial velocity of the swimmers. The walls of the boxes consisted of stationary disks of the same size as the swimmers.

The position and the velocity of the swimmers are estimated from the net force on each swimmer. A linked list algorithm [43] is used to reduce the computational effort while calculating the forces. The acceleration of an individual swimmer is calculated first from the net force, by dividing the force with the mass of the particle. The velocity-Verlet algorithm [44] is used to numerically integrate the position and the velocity. The procedure is detailed in our earlier work [38].

The major dimensionless groups that govern the dynamics of the system are χ, $\bar{L} = \frac{L}{d}$, and $\bar{k} = \frac{k_n d}{m\beta}$, where χ is the ratio of the two force scales: alignment force ($\vec{F}_a$) and forces created due to the self-propelled thrust ($\vec{F}_{\rm sp}$). The scale associated with the forces are $F_a \sim C_v d\sqrt{\beta L}$ and $F_{\rm sp} \sim m\beta$. Here, $\sqrt{\beta L}$ scales the maximum possible speed of the swimmers in each box. The expression of $\chi = \bar{L}\frac{F_a}{F_{\rm sp}}$ upon simplification can be obtained as

$$\chi = \frac{C_v L\sqrt{L}}{m\sqrt{\beta}}. \tag{8}$$

Conceptually, χ characterizes the effect of the alignment force and the self-propelled thrust force. Therefore, we have described all our results in terms of χ to identify the competition between these forces. In this work, we have varied χ by changing C_v while keeping other parameters constant. Although in a few cases we have changed the value of β of the swimmers in box 2, for simplicity we have used the β value of box 1 (which is constant throughout) for obtaining dimensionless quantities. It should be noted that, low χ or C_v values signify higher thrust force in comparison to the alignment force. With the increase of χ or C_v, the alignment force that dictates the transition of the swimmers from the random fluctuating state to an ordered collective motion increases.

Mixing calculation

A mixing parameter (η) is defined based on the correlation of the swimmer's position with respect to the initial position. The procedure followed here is similar to that of the weak sense mixing parameter of Doucet *et al.* [45]. As the swimmers' sizes are fixed, the particle size distribution at any time instant is independent of the initial distribution. The mixing calculation is done based on the swimmers' position data using principal component analysis (PCA) [38,45]. In the present problem, the following steps are used for calculating the mixing index.

(i) Based on the initial variance and mean, all swimmers' initial positions are scaled at the initial instant, $t = 0$.

(ii) The Swimmers' positions at time t are scaled based on the instantaneous variance and mean.

(iii) The correlation matrix $\rho({X_m}^t, {X_n}^0)$, where $m = 1$ and 2, and $n = 1$ and 2, is determined X_1 and X_2 are N-dimensional vectors of the x and y coordinates of the swimmers (N being the total number of swimmers). The correlation matrix involves the product of the transpose of $({X_m}^t)$ and $({X_n}^0)$, where t and 0 denote the current and initial time instants, respectively.

(iv) The correlation matrix C is formed, by assigning $C_{mn} = \rho({X_m}^t, {X_n}^0)$.

(v) The symmetric matrix M is computed, such that $M = CC^T$.

(vi) The eigenvalue problem $M\alpha = \lambda\alpha$ is solved. Here, the maximum eigenvalue is λ and the corresponding eigenvector is α.

(vii) The mixing parameter for two-dimensional space is defined as

$$\eta = \sqrt{\lambda/2}. \tag{9}$$

III. RESULTS AND DISCUSSION

We performed the simulations for different packing fractions (Ω) of swimmers. We considered two cases based on the initial packing of the swimmers in each box: 74.62% and 34.45%. In each case, the same number of swimmers were packed in the two boxes initially. Depending on χ and β, the overall mixing of the two boxes changes. The simulations are done for χ ranging from 121 to 6039. To see the effect of the swimmers' activity on mixing, we also changed the value of β in box 2.

Figure 2 illustrates the transience of mixing at different values of χ, for $\Omega = 74.62\%$. Only three representative χ values are shown in Fig. 2. Initially the swimmers are separated in two different boxes. In the earlier studies [12], due to the presence of the hydrodynamic interaction of the particles with the medium it was observed that with increasing χ the average velocity of the particles decreases due to higher damping. It was also observed that the particles move into a rotational phase and show an organized motion. In the present study where there is no damping effect, at $\chi = 604$ few swimmers move into the other box through the connecting path. At higher χ, as the average velocity of the swimmers is low, the swimmers did not jam the connecting path. Due to the higher centrifugal forces [12], a hollow core forms at the center of each box (see video SM1 in the Supplemental Material [46] for $\Omega = 74.62\%$). With further increase of χ, an oscillatory motion of the swimmers is observed in each of the boxes (see video SM2 in the Supplemental Material [46] and Fig. 2 for $\chi = 6039$ for $\Omega = 74.62\%$). Due to very slow motion of the swimmers, the mixing parameter also decreases.

Velocity vectors of the swimmers for different χ are shown in Fig. 3. At $\chi = 121$, random thermal motion of the swimmers can be seen. With the increase of χ, the alignment force increases, which helps in the alignment of the swimmers. As shown earlier in Fig. 2, at $\chi = 604$ a hollow core forms at the respective centers of the boxes and the swimmers rotate around it. It should be noted that the size of the core changes with time and at a particular instant the core sizes are different for the two boxes. With further increase of χ, the swimmers show an oscillatory pattern in one box and rotation in the other box. As can be seen from Fig. 3 for $\chi = 6039$, the left box shows oscillatory behavior of the swimmers. It should be noted that the direction of rotation (in the rotary phase) of the swimmers in any box is random. With multiple realization it is expected to see both clockwise and anticlockwise motion of the swimmers in the same box. It can be seen from Fig. 3 that at $\chi = 604$ the swimmers are rotating in the anticlockwise direction in box 2, whereas the motion is clockwise at $\chi = 3623$ in the same box. Things become more interesting when

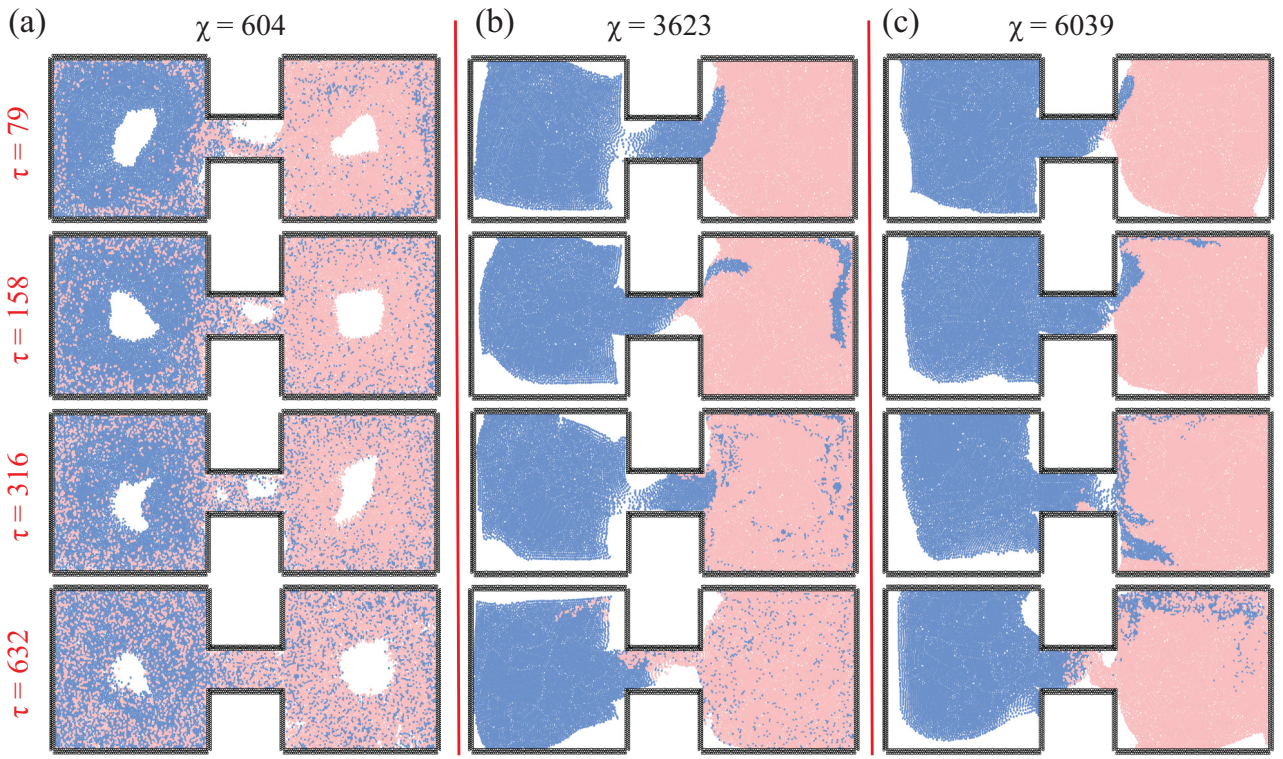

FIG. 2. Mixing of swimmers within the domain at different nondimensionalized times $\tau = t/\sqrt{\frac{L}{\beta}}$ and χ for $\Omega = 74.62\%$. Swimmers of box 1 and box 2 are colored with blue and pink, respectively. (a) At $\chi = 604$, a hollow core is formed that changes its position and size with time. The connection between the two boxes get established and mixing is observed. The swimmers inside the boxes are rotating in the opposite directions. (b) At $\chi = 3623$, a mixed mode of oscillation and rotation is observed. (c) At $\chi = 6039$, the motion of the swimmers is slower.

the boxes are filled with swimmers with different activity. This is studied through having a higher thrust coefficient β. As a case study, β in box 2 is set to 10 times more than β in box 1. The collective behavior of the swimmers at different χ is shown in Fig. 4 for $\Omega = 74.62\%$. Because of the higher β, the swimmers in box 2 are more active than those in box 1. At $\chi = 604$, more active swimmers from box 2 move into box 1 and block the connecting path. It can be seen from Fig. 4, at $\tau = 79$ the swimmers from box 2 move into box 1 and restrict the motion of the swimmers in box 1. The higher activity of the swimmers of box 2 creates this jammed state in box 1, whereas the swimmers in box 2 are in a rotary state. As time progresses, more swimmers from box 2 penetrate box 1 and create a rotating "wheel," whereas all other swimmers in box 1 are stationary (see video SM3 in the Supplemental Material [46]). At higher χ and sufficiently longer time, the swimmers of box 2 form smaller groups inside box 1. At $\chi = 6039$, the swimmers in box 1 are oscillating like a single entity whereas, the swimmers in box 2 are rotating. The behavior of the swimmers is quite similar to that of the cases explained earlier where all the swimmers are in a similar activity state.

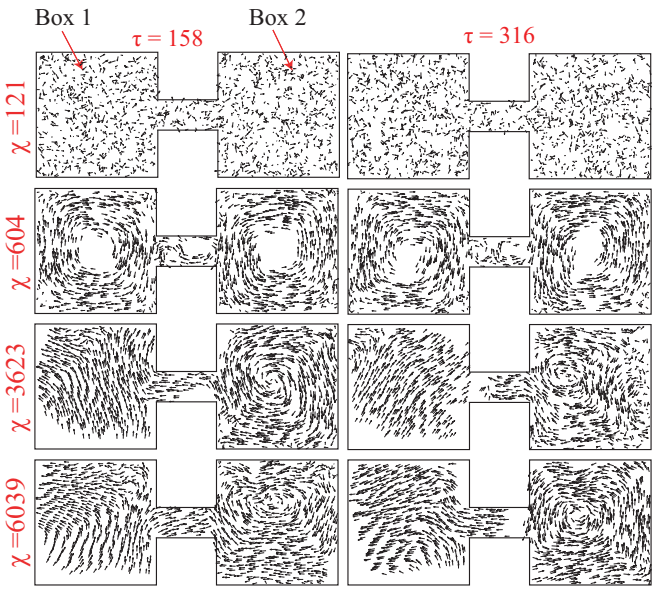

FIG. 3. Velocity vectors at different time instants for different χ for $\Omega = 74.62\%$. At very low χ, random motion of the swimmers is observed and at higher χ the motions are ordered. A few velocity vectors are skipped for better clarity of the image.

Mixing of swimmers for $\Omega = 34.45\%$ at $\tau = 632$ for different χ is shown in Fig. 5. As shown in Fig. 5, at lower χ the swimmers are either in a rotational state with a hollow core in both the boxes [see Fig. 5(a) for $\chi = 604$] or in a rotational state with a filled core [see Fig. 5(b) for $\chi = 604$]. Generally, the direction of rotations is opposite in the two boxes. For $\chi = 3623$, when β is set to 1 in both the boxes, mixing characteristics are different in the two boxes. It can be seen from Fig. 5(a) that for $\chi = 3623$ mixing is better in the right box (box 2). The effects of the packing fraction of the

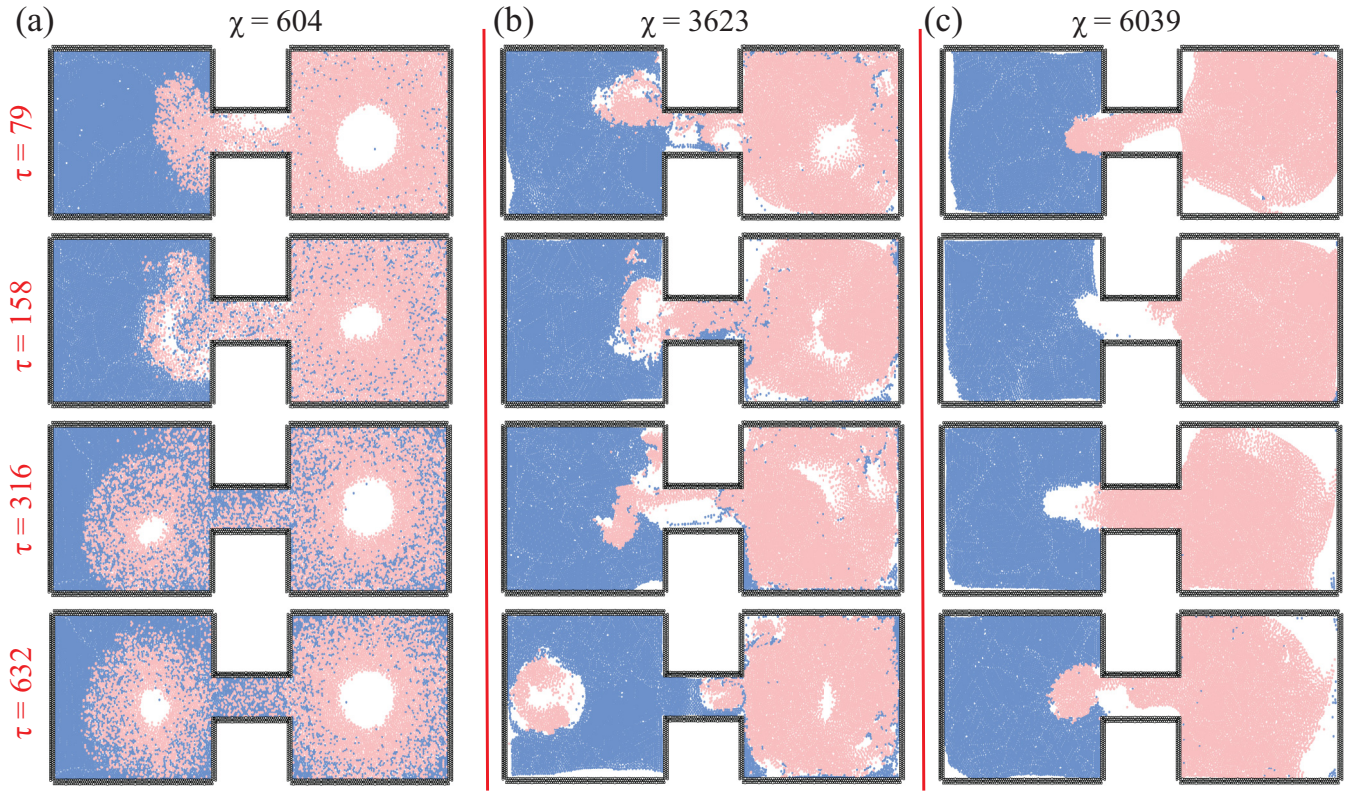

FIG. 4. Mixing of swimmers within the domain at different nondimensionalized time $\tau = t/\sqrt{\frac{L}{\beta}}$ and χ for $\Omega = 74.62\%$. Swimmers of box 1 and 2 are colored with blue and pink, respectively. The self-propelled coefficient β is set to 10 for the right box and it is 1 for the left box. (a) At $\chi = 302$, swimmers are in the jammed state in the left box, whereas they are rotating in the right box. (b) At $\chi = 3623$, a hollow core is formed that changes its position and size with time. The connection between the two boxes is established and mixing is observed. (c) At $\chi = 6039$, the pattern formed by the swimmers is similar to that at $\chi = 3623$. However, the average velocity of the swimmers is much slower.

swimmers are visible from the figures. In $\Omega = 34.45\%$, the disconnected motion of the swimmers is observed, whereas, due to the higher packing fraction in $\Omega = 74.62\%$, there are always a few swimmers in the connecting path. When the β value of the swimmers in the right box is 10 times that of the swimmers in the left box, the mixing of the swimmers enhances and several smaller flocks are observed. For $\chi = 3623$ and 6039 in Fig. 5(b), an oscillatory motion is observed inside the connecting pathway of the two boxes and in the left box (box 1).

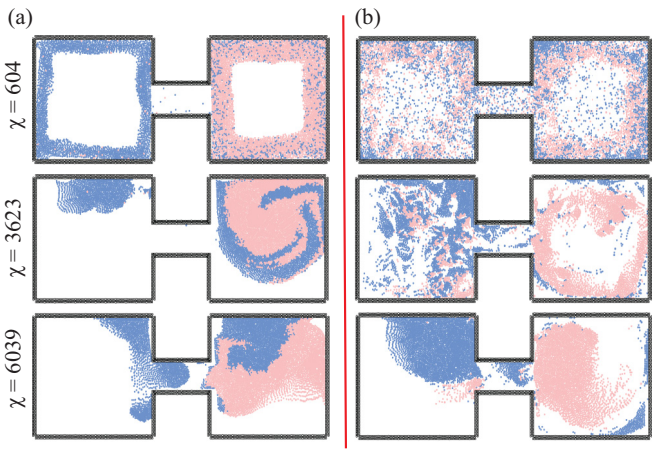

FIG. 5. Mixing of swimmers for different χ values for $\Omega = 34.45\%$. (a) The β value is the same for all the swimmers in the two boxes ($\beta = 1$). (b) The β value of the swimmers in the right box is 10 times that of the swimmers in the left box. Corresponding time $\tau = 632$.

A. Order parameter

To describe the flocking behavior of the swimmers, the order parameter ϕ has been defined as [23,24,47]

$$\phi = \left| \frac{1}{N} \sum_{i=1}^{N} \frac{\vec{v}_i}{|\vec{v}_i|} \right|, \tag{10}$$

where $\vec{v}_i$ represents the velocity of the ith swimmer and N is the total number of the swimmers. In the current work, the time-averaged order parameter Φ of the flock increases with increasing χ (see Fig. 6). This is mainly due to two factors: the effect of the confinement and the type of aggregation formed. Because of these factors, three distinct regimes of the swimmers are observed for different χ (see Fig. 6). As shown in Fig. 6(a), three distinct regimes are observed for $\Omega = 74.62\%$: thermal, rotational, and oscillatory. There is also a transitional regime where the swimmers show the behavior of both the rotational and the oscillatory phases. Thermal motion is observed at $\chi = 121$, where the value of the order parameter is the lowest. With the increase of χ the ordering

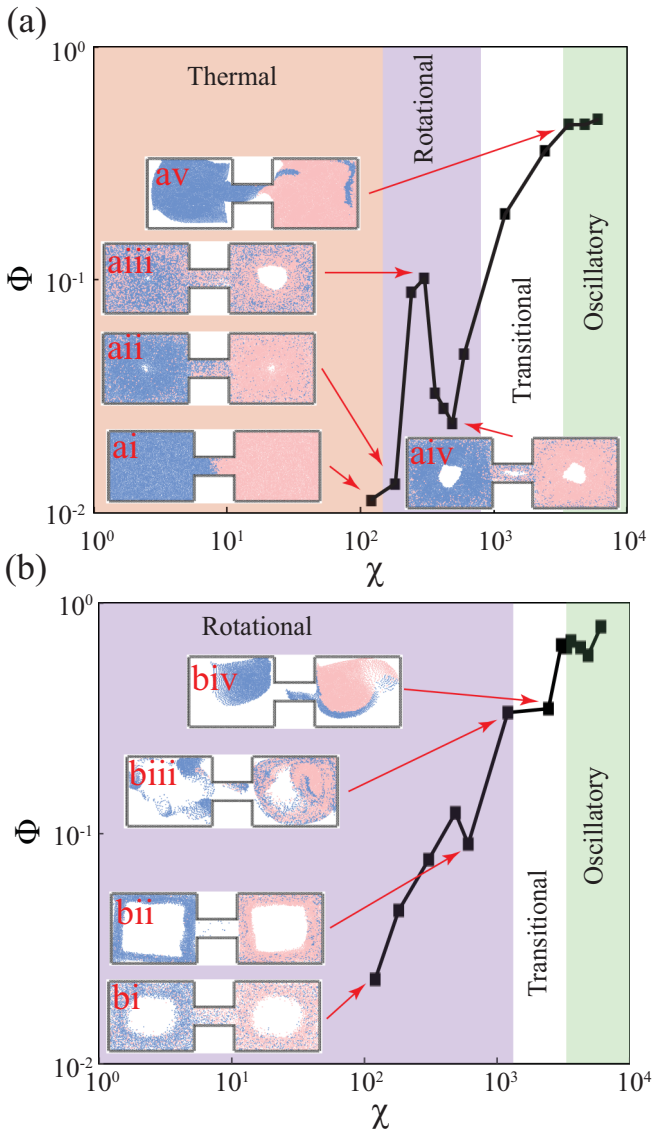

FIG. 6. The temporally averaged order parameter Φ is plotted for increasing χ values. (a) Φ is plotted for $\Omega = 74.62\%$. Three distinct regimes can be seen: thermal, rotational, and oscillatory. For certain χ values a transitional regime between the rotational and oscillatory regimes is also observed. (b) Φ is plotted for $\Omega = 34.45\%$. Thermal motion is not observed here even for the smaller $\chi = 121$. All subfigures correspond to $\tau = 158$.

increases and the swimmers start showing a rotational phase. At the beginning of this rotational regime, the swimmers start rotating in the two boxes, although there is no movement of the swimmers in the connecting path. The representative image (subfigure aii) is shown in the inset of Fig. 6(a). Thus, the order parameter is lower, and it increases sharply with the increase of χ. The order parameter is maximum when all the swimmers are in motion (subfigure aiii). Inside the rotational regime, the value of the order parameter decreases because of the formation of smaller flocks (see the connecting path of subfigure aiv). With a further increase of χ the activity of the swimmers dies down, and they start oscillating inside the boxes (for $\chi > 3623$). It should be noted that the increase of Φ does not indicate higher velocity of the flocks.

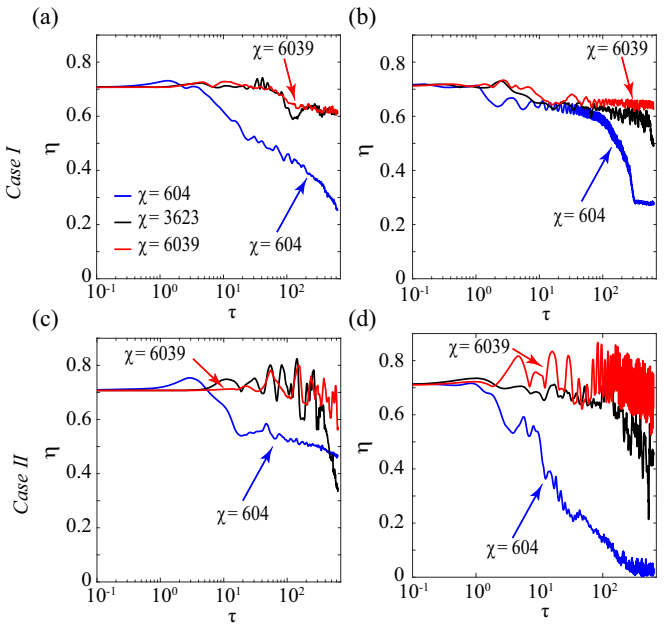

FIG. 7. The mixing parameter for different χ values for different cases. In the first column of the figure [panels (a) and (c)], the β value is same for all the swimmers in the two boxes ($\beta = 1$). In the second column [panels (b) and (d)], the β value in the right box is 10 times that in the left box.

With the decrease of the packing fraction of the swimmers ($\Omega = 34.45\%$), surprisingly, the thermal motion is not observed. Only rotational and oscillatory regimes are observed. Rotational motions can be seen in the inset (subfigure bi) of Fig. 6(b) for $\chi = 121$. The order parameter increases with the increase in χ. A small decrease in the order parameter is observed for $\chi = 604$, when there are no swimmers in the connecting path (see subfigure bii). With further increase in χ the swimmers are forming smaller flocks, although there exists a bulk motion (see subfigure biii). Similar to the $\Omega = 74.62\%$, here also a transitional regime exists between the rotational and the oscillatory phases. In the transitional phase, either the swimmers in both the boxes are rotating with oscillation or there is oscillation in one box and rotation in the other. It should be noted that for both cases, the increase of the order parameter does not suggest higher mixing. In most of the cases, the mixing is reduced with the increase of the order parameter, particularly at higher χ.

B. Quantification of mixing

To quantitatively identify mixing, we defined the mixing parameter η as described in Sec. II. It should be noted that the lower value of η signifies better mixing. Figure 7 shows the variation of η as a function of time for different χ values for different cases studied here. When the thrust coefficient is the same for all the swimmers in boxes 1 and 2, the mixing parameter is higher (i.e., low η) at $\chi = 604$, as shown in Fig. 7(a). At $\chi = 3623$, the mixing parameter decreases mainly due to the oscillatory behavior of the swimmers. The mixing parameters for $\chi = 3623$ and 6039 are also similar. Our objective in this work is to show the mixing of self-propelled swimmers and

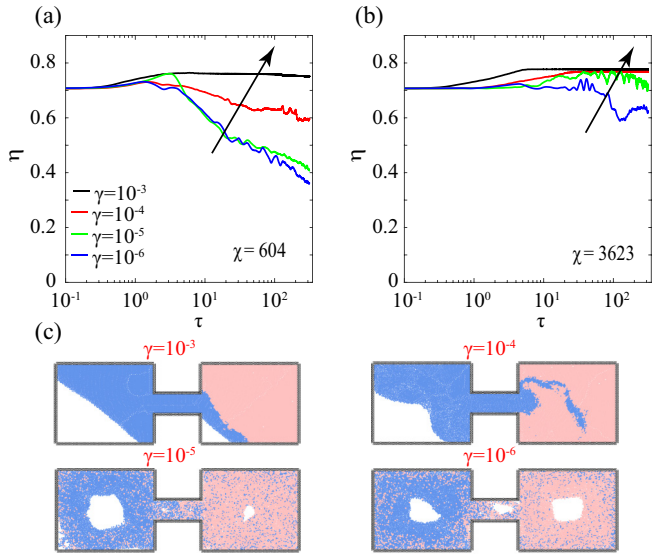

FIG. 8. The mixing parameter for different χ values for different γ for $\Omega = 74.62\%$. (a) Effect of γ is shown for $\chi = 604$. (b) The effect of γ is shown for $\chi = 3623$. With the increase of γ the mixing parameter increases. The arrow indicates the direction of the increase of γ. (c) Mixing of swimmers for different γ for $\chi = 604$. With the increase of γ, the rotational phase to the jammed state phase transition is observed.

not to identify the best mixing criteria based on β and χ. When the thrust coefficient is higher in box 2, as shown in Fig. 7(b), the higher activity of the swimmers enhances the mixing of the swimmers of $\chi = 3623$. In general, due to the increase in friction and higher alignment forces, the mixing parameter decreases with an increase in χ.

It is also interesting to see the effect of the packing fraction of the swimmers in the mixing process. Earlier, it was observed that the velocity of the particle decreases with an increase in the volume fraction of the swimmers [48]. Thus, it is expected that the mixing behavior will change with the swimmers' packing fraction Ω. Mixing behaviors of the swimmers are shown in Figs. 7(c) and 7(d) for $\Omega = 34.45\%$. When β is the same for all the particles in the two boxes ($\beta = 1$), the mixing parameter increases with χ up to $\chi = 3623$ and then decreases. When β in the right box is 10 times that in the left box, it can be seen from Fig. 7(d) that the mixing behavior is almost similar to that with $\Omega = 74.62\%$ for $\chi = 6039$ and 3623. It can be seen from Fig. 7(d) that the mixing parameter for $\chi = 604$ is maximum. The higher active swimmers from box 2 help in moving the swimmers of the left box (box 1). Therefore, it can be expected that, with the increase of β, the mixing parameter will increase particularly for higher χ.

C. Effect of noise

In order to identify the effect of the white noise term in the overall mixing of the swimmers, different values of noise amplitudes (γ) are chosen. As seen from Fig. 8, the mixing parameter (η) is a strong function of γ. For $\chi = 604$, the variation is more prominent compared to the higher χ values. With the increase of the value of γ the overall dynamics of the swimmers changes. As shown in Fig. 8(c), at higher γ values the swimmers are not able to move and exhibit a jammed state, whereas at lower values ($\leqslant 10^{-5}$) the swimmers are able to move freely. Phase transitions because of the noise have also been observed earlier by Ginelli *et al.* [19].

IV. CONCLUSION

Phase transition and mixing of self-propelled swimmers are studied in this work. Different phases of the swimmers, from the random motion to the rotary state, are identified. Activity-induced mixing of the swimmers inside an enclosed chamber is characterized by the mixing index. The thrust coefficient and the alignment forces dictate the phase transition and the mixing of the swimmers.

Phase transitions and mixing indexes were identified for different packing fractions of the swimmers. It is observed that for very high packing fractions of ∼75% the swimmers show thermal, rotational, and oscillatory phases. For lower packing fractions the thermal motion is missing and the swimmers are mostly in the rotational state. Mixing of the swimmers is quantitatively identified by using a mixing parameter. The general observation on mixing is that the mixing parameter decreases with the increase of χ. It is also observed that, with the presence of more active swimmers (higher β) in box 2, the mixing is faster and better at lower χ, whereas the effect of β is not very significant at lower χ, except at a low packing fraction.

ACKNOWLEDGMENTS

The first author acknowledges financial support from the New Faculty Initiative Grant of the Indian Institute of Technology Madras under Grant No. MEE171861/NFIGPALL. The authors acknowledge the reviewers for critical remarks and suggestions to improve the quality of the manuscript.

[1] I. D. Couzin, J. Krause, R. James, G. D. Ruxton, and N. R. Franks, Collective memory and spatial sorting in animal groups, J. Theor. Biol. **218**, 1 (2002).

[2] J. L. Silverberg, M. Bierbaum, J. P. Sethna, and I. Cohen, Collective Motion of Humans in Mosh and Circle Pits at Heavy Metal Concerts, Phys. Rev. Lett. **110**, 228701 (2013).

[3] C. Dombrowski, L. Cisneros, S. Chatkaew, R. E. Goldstein, and J. O. Kessler, Self-Concentration and Large-Scale Coherence in Bacterial Dynamics, Phys. Rev. Lett. **93**, 098103 (2004).

[4] I. H. Riedel, K. Kruse, and J. Howard, A self-organized vortex array of hydrodynamically entrained sperm cells, Science **309**, 300 (2005).

[5] J. Deseigne, O. Dauchot, and H. Chaté, Collective Motion of Vibrated Polar Disks, Phys. Rev. Lett. **105**, 098001 (2010).

[6] I. Theurkauff, C. Cottin-Bizonne, J. Palacci, C. Ybert, and L. Bocquet, Dynamic Clustering in Active Colloidal Suspensions with Chemical Signaling, Phys. Rev. Lett. **108**, 268303 (2012).

[7] M. C. Marchetti, J. F. Joanny, S. Ramaswamy, T. B. Liverpool, J. Prost, M. Rao, and R. A. Simha, Hydrodynamics of soft active matter, Rev. Mod. Phys. **85**, 1143 (2013).

[8] A. Bricard, J. B. Caussin, N. Desreumaux, O. Dauchot, and D. Bartolo, Emergence of macroscopic directed motion in populations of motile colloids, Nature (London) **503**, 95 (2013).

[9] J. B. Caussin, A. Solon, A. Peshkov, H. Chaté, T. Dauxois, J. Tailleur, V. Vitelli, and D. Bartolo, Emergent Spatial Structures in Flocking Models: A Dynamical System Insight, Phys. Rev. Lett. **112**, 148102 (2014).

[10] A. Baskaran and M. C. Marchetti, Statistical mechanics and hydrodynamics of bacterial suspensions, Proc. Natl. Acad. Sci. U.S.A. **106**, 15567 (2009).

[11] X. Yang, M. L. Manning, and M. C. Marchetti, Aggregation and segregation of confined active particles, Soft Matter **10**, 6477 (2014).

[12] P. S. Mahapatra, A. Kulkarni, S. Mathew, M. V. Panchagnula, and S. Vedantam, Transitions between multiple dynamical states in a confined dense active-particle system, Phys. Rev. E **95**, 062610 (2017).

[13] A. A. Al Sayegh, L. Klushin, and J. Touma, Steady and transient states in low-energy swarms: Stability and first-passage times, Phys. Rev. E **93**, 032602 (2016).

[14] A. C. H. Tsang and E. Kanso, Circularly confined microswimmers exhibit multiple global patterns, Phys. Rev. E **91**, 043008 (2015).

[15] A. Czirók, A.-L. Barabási, and T. Vicsek, Collective Motion of Self-Propelled Particles: Kinetic Phase Transition in One Dimension, Phys. Rev. Lett. **82**, 209 (1999).

[16] C. W. Reynolds, Flocks, herds and schools: A distributed behavioral model, Comput. Graph. **21**, 25 (1987).

[17] T. Vicsek, A. Czirók, E. L. Ben-Jacob, I. Cohen, and O. Shochet, Novel Type of Phase Transition in a System of Self-Driven Particles, Phys. Rev. Lett. **75**, 1226 (1995).

[18] A. Baskaran and M. C. Marchetti, Hydrodynamics of self-propelled hard rods, Phys. Rev. E **77**, 011920 (2008).

[19] F. Ginelli, F. Peruani, M. Bär, and H. Chaté, Large-Scale Collective Properties of Self-Propelled Rods, Phys. Rev. Lett. **104**, 184502 (2010).

[20] A. P. Solon, H. Chaté, and J. Tailleur, From Phase to Microphase Separation in Flocking Models: The Essential Role of Nonequilibrium Fluctuations, Phys. Rev. Lett. **114**, 068101 (2015).

[21] J. Bialké, T. Speck, and H. Löwen, Crystallization in a Dense Suspension of Self-Propelled Particles, Phys. Rev. Lett. **108**, 168301 (2012).

[22] S. Henkes, Y. Fily, and M. C. Marchetti, Active jamming: Self-propelled soft particles at high density, Phys. Rev. E **84**, 040301 (2011).

[23] T. Vicsek and A. Zafeiris, Collective motion, Phys. Rep. **517**, 71 (2012).

[24] S. Pattanayak and S. Mishra, Collection of polar self-propelled particles with a modified alignment interaction, J. Phys. Commun. **2**, 045007 (2018).

[25] D. O. Pushkin and J. M. Yeomans, Fluid Mixing by Curved Trajectories of Microswimmers, Phys. Rev. Lett. **111**, 188101 (2013).

[26] X. L. Wu and A. Libchaber, Particle Diffusion in a Quasi-Two-Dimensional Bacterial Bath, Phys. Rev. Lett. **84**, 3017 (2000).

[27] M. J. Kim and K. S. Breuer, Enhanced diffusion due to motile bacteria, Phys. Fluids **16**, L78 (2004).

[28] G. L. Miño, J. Dunstan, A. Rousselet, E. Clément, and R. Soto, Induced diffusion of tracers in a bacterial suspension: Theory and experiments, J. Fluid Mech. **729**, 423 (2013).

[29] P. T. Underhill, J. P. Hernandez-Ortiz, and M. D. Graham, Diffusion and Spatial Correlations in Suspensions of Swimming Particles, Phys. Rev. Lett. **100**, 248101 (2008).

[30] Z. Lin, J.-L. Thiffeault, and S. Childress, Stirring by squirmers, J. Fluid Mech. **669**, 167 (2011).

[31] W. K. Dewar, R. J. Bingham, R. L. Iverson, D. P. Nowacek, L. C. St. Laurent, and P. H. Wiebe, Does the marine biosphere mix the ocean? J. Mar. Res. **64**, 541 (2006).

[32] A. Sokolov, R. E. Goldstein, F. I. Feldchtein, and I. S. Aranson, Enhanced mixing and spatial instability in concentrated bacterial suspensions, Phys. Rev. E **80**, 031903 (2009).

[33] D. L. Koch and G. Subramanian, Collective hydrodynamics of swimming microorganisms: Living fluids, Annu. Rev. Fluid Mech. **43**, 637 (2011).

[34] J. J. Molina, Y. Nakayama, and R. Yamamoto, Hydrodynamic interactions of self-propelled swimmers, Soft Matter **9**, 4923 (2013).

[35] Q.-S. Chen and Y.-Q. Ma, Collective motion of self-propelled particles with density-dependent switching effect, AIP Adv. **6**, 055024 (2016).

[36] H. Levine, W.-J. Rappel, and I. Cohen, Self-organization in systems of self-propelled particles, Phys. Rev. E **63**, 017101 (2000).

[37] E. Mones, A. Czirók, and T. Vicsek, Anomalous segregation dynamics of self-propelled particles, New J. Phys. **17**, 063013 (2015).

[38] P. S. Mahapatra, S. Mathew, M. V. Panchagnula, and S. Vedantam, Effect of size distribution on mixing of a polydisperse wet granular material in a belt-driven enclosure, Granular Matter **18**, 1 (2016).

[39] D. F. Hinz, A. Panchenko, T. Y. Kim, and E. Fried, Motility versus fluctuations in mixtures of self-motile and passive agents, Soft Matter **10**, 9082 (2014).

[40] C. Drumm, S. Tiwari, J. Kuhnert, and H. Bart, Finite pointset method for simulation of the liquid–liquid flow field in an extractor, Comput. Chem. Eng. **32**, 2946 (2008).

[41] H. Kunz and C. K. Hemelrijk, Simulations of the social organization of large schools of fish whose perception is obstructed, Appl. Anim. Behav. Sci. **138**, 142 (2012).

[42] J. Demšar, C. K. Hemelrijk, H. Hildenbrandt, and I. L. Bajec, Simulating predator attacks on schools: Evolving composite tactics, Ecol. Model. **304**, 22 (2015).

[43] S. Plimpton, Fast parallel algorithms for short-range molecular dynamics, J. Comput. Phys. **117**, 1 (1995).

[44] W. C. Swope, H. C. Andersen, P. H. Berens, and K. R. Wilson, A computer simulation method for the calculation of equilibrium constants for the formation of physical clusters of molecules: Application to small water clusters, J. Chem. Phys. **76**, 637 (1982).

[45] J. Doucet, F. Bertrand, and J. Chaouki, A measure of mixing from Lagrangian tracking and its application to granular and fluid flow systems, Chem. Eng. Res. Design **86**, 1313 (2008).

[46] See Supplemental Material at http://link.aps.org/supplemental/10.1103/PhysRevE.99.012609 for video SM1, rotary phase of the active swimmers at $\chi = 604$; video SM2, oscillatory phase of the active swimmers at $\chi = 6039$; and video SM3, at $\chi = 604$ where higher active swimmers are present in box 2.

[47] A. Cavagna, A. Cimarelli, I. Giardina, G. Parisi, R. Santagati, F. Stefanini, and M. Viale, Scale-free correlations in starling flocks, Proc. Natl. Acad. Sci. U.S.A. **107**, 11865 (2010).

[48] I. Llopis and I. Pagonabarraga, Dynamic regimes of hydrodynamically coupled self-propelling particles, Europhys. Lett. **75**, 999 (2006).